Photochemistry and Photobiology, 2012, 88: 527–536

Porphyrin-Cellulose Nanocrystals: A Photobactericidal Material that Exhibits Broad Spectrum Antimicrobial Activity†

Bradley L. Carpenter[1], Elke Feese[1], Hasan Sadeghifar[2], Dimitris S. Argyropoulos[1,2,3] and Reza A. Ghiladi*[1]

[1]Department of Chemistry, North Carolina State University, Raleigh, NC
[2]Department of Forest Biomaterials, North Carolina State University, Raleigh, NC
[3]Department of Chemistry, University of Helsinki, Helsinki, Finland

Received 7 October 2011, accepted 7 February 2012, DOI: 10.1111/j.1751-1097.2012.01117.x

ABSTRACT

Towards our overall objectives of developing potent antimicrobial materials to combat the escalating threat to human health posed by the transmission of surface-adhering pathogenic bacteria, we have investigated the photobactericidal activity of cellulose nanocrystals that have been modified with a porphyrin-derived photosensitizer (PS). The ability of these previously synthesized porphyrin-cellulose-nanocrystals (CNC-Por (1)) to mediate bacterial photodynamic inactivation was investigated as a function of bacterial strain, incubation time and illumination time. Despite forming an insoluble suspension, CNC-Por (1) showed excellent efficacy toward the photodynamic inactivation of *Acinetobacter baumannii*, multidrug-resistant *Acinetobacter baumannii* (MDRAB) and methicillin-resistant *Staphylococcus aureus* (MRSA), with the best results achieving 5–6 log units reduction in colony forming units (CFUs) upon illumination with visible light (400–700 nm; 118 J cm^{-2}). CNC-Por (1) mediated the inactivation of *Pseudomonas aeruginosa*, although at reduced activity (2–3 log units reduction). Confocal laser scanning microscopy of CNC-Por (1) after incubation with *A. baumannii* or *S. aureus* suggested a lack of internalization of the PS. Research into alternative materials such as CNC-Por (1) may lead to their application in hospitals and healthcare-related industries wherein novel materials with the capability of reducing the rates of transmission of a wide range of bacteria, particularly antibiotic resistant strains, are desired.

INTRODUCTION

The increasing prevalence of antibiotic-resistant bacteria has led to a rapidly emerging need to develop new strategies to mitigate nosocomial infections which are mediated by the survival of pathogenic bacteria on surfaces. Such hospital acquired infections (HAIs) now infect one of every 20 hospitalized patients, and, as the cause of approximately 100 000 deaths annually in the United States alone, represent the sixth leading cause of mortality in the United States and an increasing economic burden on an already strained healthcare system (1). The pathogens that give rise to HAIs are capable of surviving for prolonged periods in hospital environments (linens, drapes, bed rails) and on the hands and clothes of healthcare workers (2–4). Depending on the strain, *Acinetobacter baumannii*, *Mycobacterium tuberculosis* and *Staphylococcus aureus* (as examples of bacteria that are of interest to this specific lab) all have been shown to remain viable on dry, abiotic surfaces for upwards of 4–7 months (5). Surfaces that are not effectively disinfected can lead to the proliferation of pathogens and transmission to hosts, thereby necessitating research into the next generation of materials that possess antimicrobial properties.

Antimicrobial photodynamic therapy (aPDT) (6–8) has emerged as an alternative strategy for the treatment of microbial infections. aPDT employs a photosensitizer (PS) that generates reactive oxygen species (i.e. radicals or singlet oxygen ($^1O_2$)) upon illumination with visible or near infrared light. $^1O_2$ possesses a number of unique characteristics that make it amenable for antimicrobial applications. These include damaging reactivity with most biomolecules (9–16), a short lifetime of $\sim 10^{-6}$ s in aqueous environments (17), and the formation of a harmless byproduct when left unreacted (ground state molecular oxygen). Additionally, a number of studies have shown that aPDT is equally effective against both drug-susceptible and drug-resistant bacterial strains (7,18–20), making it a particularly attractive treatment for bacterial infections. While significant efforts have focused on the application of aPDT for the treatment of bacterial infections *in vivo*, a number of more recent studies have demonstrated that photobactericidal materials may have widespread applicability for the elimination of bacteria prior to infection. Specifically, it has been shown that PSs are capable of mediating the photodynamic inactivation (PDI) of bacteria when incorporated, either through covalent or noncovalent conjugation, into a number of different materials (films (21–23), membranes (24), polymers (25,26), nanoparticles (27,28) and fabrics (29–31)). Reactive oxygen species have been shown to diffuse over a wide range of distances (from < 250 nm for $^1O_2$ to ~ 1.5 mm for H_2O_2) in aqueous solution (32–34), allowing the potential for the effective inactivation of bacteria on wet surfaces when the PS is within sufficient proximity to the pathogen. Photobactericidal surfaces generated from the covalent attachment of PSs to a solid support may possess a number of advantages over other antimicrobial materials that incorporate compounds derived from biomolecules (antimicrobial peptides, natural products) (35–38), cationic species

†This paper is part of the Symposium-in-Print on "Antimicrobial Photodynamic Therapy and Photoinactivation."

*Corresponding author email: reza_ghiladi@ncsu.edu (Reza A. Ghiladi)

(quarternary ammonium, pyridinium, or phosphonium salts) (39–45), organic compounds (conventional antibiotics, phenolics, *N*-halamines, biguanides) (46–50), or heavy metals (copper, silver and zinc) (46,51,52). These advantages include employing reactive oxygen species as the biocidal agents (which, given their short lifetimes and decay to relatively unreactive end products, can be considered environmentally benign), permanent attachment of the PS through covalent conjugation, and the ability of the PS to potentially function in the absence of direct contact with the bacterium. Additionally, as $^1O_2$ or other reactive oxygen species may cause nonspecific damage, photodynamic materials possess antiviral (53,54), antifungal (55,56) and antiparasitic (57–59) properties. Finally, as PDI employs harmless white light, it has the advantage over UVC (as an example of another light-based sterilization technique) in that it can function without the need for protecting people against the deleterious effects of long-term or high-intensity UV exposure.

As a potential solid support for photobactericidal materials, cellulose possesses a number of chemical and physical properties that have been well characterized (60). It is the most naturally abundant biomaterial on the planet, and represents a structural motif upon which the bulk material of our plant systems and a number of derivative biopolymers (e.g. chitin) are based. Cellulose is comprised of very regular crystalline units or nanodomains that, upon acid hydrolysis (61–63), yield highly crystalline rod-like hydrophilic particles at the nanoscale level (100–400 nm in length (60)) that possess high mechanical strength and enhanced properties when compared with other polymers (64). For example, these cellulose nanocrystals (CNC) possess a high melting temperature that may positively affect the thermal transition properties of any covalently attached functional groups on them, a very attractive proposition in designing high melt composites, thermal extrusions and temperature-resistant materials (60,64). While cellulose nanocrystals have been explored mainly for their contributions to macroscopic properties of bulk materials, they also possess a number of unique molecular characteristics of significance that allow them to act as scaffolds for nanomaterials (60,64–66). These include: (1) taking the form of rigid molecular rods of well-defined dimensions; (2) enantiopurity with embedded polymeric directionality; and (3) an etched molecular pattern on their surfaces composed of primary hydroxyl groups at the C_6 position which are amenable to chemical modification. Thus, cellulose is a readily abundant, renewable material that, when combined with these attractive chemical features in one system, provides a unique paradigm for chemical transformations and functionality in the design of novel photobactericidal materials.

Previously, we described the synthesis and characterization of CNC-Por (**1**) (67), a photobactericidal material formed from the covalent attachment of an alkyne-containing porphyrin PS to the surface of azide-modified cellulose nanocrystals using the Cu(I)-catalyzed Huisgen-Meldal-Sharpless 1,3-dipolar cycloaddition reaction (Fig. 1). While the focus of that report was primarily on the physico-chemical properties of CNC-Por (**1**), we also demonstrated that this material was able to mediate the photodynamic inactivation of both methicillin-susceptible *S. aureus* (MSSA) and *M. smegmatis* (as a surrogate for *M. tuberculosis*) with high efficiency, yet exhibited relatively low bactericidal activity against *E. coli*. Given the limited scope of the previous antimicrobial study in which only three strains of drug-susceptible bacteria were explored, and in order to gain insight into the mechanism of porphyrin-cellulose nanocrystals as PSs in the photoinactivation of bacteria, the focus of the present report is to further explore the potential of CNC-Por (**1**) as a photobactericidal material. In addition to supplemental characterization of **CNC-**Por (**1**) by UV–Visible spectroscopy, the antimicrobial properties of this material were investigated against *Acinetobacter baumannii*, multiple-drug resistant *Acinetobacter baumannii* (MDRAB), methicillin-resistant *Staphylococcus aureus* (MRSA) and *Pseudomonas aeruginosa*. As will be demonstrated, CNC-Por (**1**) exhibited excellent antimicrobial activity for all strains examined with the exception of *P. aeruginosa*, which was only moderately inactivated. When combined with the results of the previous investigation (67), the current study suggests that CNC-Por (**1**) is able to mediate the inactivation of the bacterial strains studied despite their varying taxonomic classification, highlighting the potential application of this photobactericidal material in inactivating microbes from contaminated surfaces given its apparent broad spectrum antimicrobial activity. Additionally, we imaged *A. baumannii* using confocal fluorescence microscopy in the presence of both CNC-Por (**1**) and the solution-based PS Zn-EpPor (**3**), the results of which will be discussed in the context of PS internalization and the mode of action of CNC-Por (**1**) in mediating antimicrobial PDI.

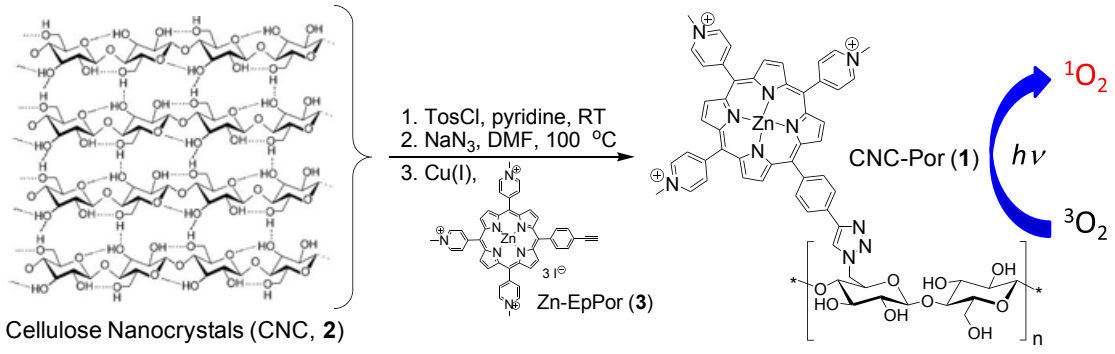

Figure 1. Synthesis of cellulose nanocrystal-porphyrin conjugate CNC-Por (**1**). For the benzoylated derivative, **1-Bz**, the structure is the same as CNC-Por (**1**) with the exception that the hydroxy groups are replaced with benzoyl esters.

MATERIALS AND METHODS

Materials. Buffer salts were purchased from Fisher Scientific, Nutrient Broth #234000 was obtained from BD Difco, LB-Miller broth from EMD Chemicals and Tryptic Soy Broth from Teknova. Polylysine solution was purchased from Sigma Aldrich. Unless otherwise specified, all other chemicals were obtained from commercial sources in the highest purity available. Ultrapure water used for all media and buffers was provided by an Easypure II system (Barnstead). High precision no. 1.5 coverslips were purchased from Bioscience Tools. All procedures were carried out under commonly practiced sterile techniques.

Preparation of CNC-Por (1). Porphyrin-cellulose nanocrystals, CNC-Por (**1**) and its benzoylated derivative, **1-Bz**, were prepared as previously described (61, 62, 66, 67). Briefly, cellulose nanocrystals (CNC, **2**) were obtained from the acid hydrolysis of cotton fibers and were subsequently treated with tosyl chloride followed by sodium azide to modify the primary hydroxyl groups for installment of surface-azide units. Covalent attachment of the alkyne-containing porphyrin Zn-EpPor (**3**) to the azide-modified cellulose nanocrystals was performed using the Cu(I)-catalyzed Huisgen-Meldel-Sharpless 1,3-dipolar cycloaddition reaction. Purification of the target compound was performed as published, resulting in the formation of CNC-Por (**1**) as an insoluble, green crystalline material. ICP-mass spectrometry, provided by the Environmental and Agricultural Testing Service (EATS) Facility (NC State University), was used to determine the concentration of Zn ions in samples of CNC-Por (**1**), which is equivalent to the porphyrin loading if complete metallation of the porphyrin is assumed. 10 mg of lyophilized CNC-Por (**1**) was digested in 10 mL of HCl, followed by heating to 60°C for ~2 h. Once digested, it was assumed that the porphyrin was fully demetallated, allowing for the Zn concentration to be determined using ICP mass spectrometry. The porphyrin loading was found to be 0.062 μmoles porphyrin/mg CNC-Por (**1**). Using this empirically determined value, a 1 mM stock solution was prepared using filter sterilized ultrapure water, and was stored in the dark at 4°C for subsequent use in the PDI assays.

UV–visible spectroscopic characterization of CNC-Por (1). UV–visible absorption spectra were collected at room temperature with a Cary 50 UV–visible spectrophotometer using quartz microcuvettes (1 cm pathlength). A stock solution of **1-Bz** and one of the precursor porphyrin Zn-EpPor (**3**) (68) were prepared in DMSO. After dilution with water to a final solution composition of 30:1 H_2O:DMSO, the UV–visible spectra were recorded. The known molar absorption coefficient of compound Por (195 $mM^{-1}cm^{-1}$) was used to normalize the spectra.

Bacterial cell culture. The bacterial strains *Acinetobacter baumannii* (ATCC #19606), multidrug resistant *Acinetobacter baumannii* (MDRAB; ATCC #BAA-1605) and methicillin-resistant *Staphylococcus aureus* (MRSA; ATCC #BAA-44) were kindly donated by Prof. Christian Melander (North Carolina State University). *Pseudomonas aeruginosa* (ATCC #97) was obtained from the American Type Culture Collection (Manassas, VA). Aliquots of each bacterial species were prepared in a 1:1 broth:glycerol ratio and stored at −80°C. *Acinetobacter baumannii* was grown in Miller LB broth without antibiotics, while the MDRAB strain was grown in Miller LB broth with 5 μg mL^{-1} tetracycline. Methicillin-resistant *S. aureus* was grown in Tryptic-Soy broth with 5 μg mL^{-1} tetracycline and *Pseudomonas aeruginosa* was grown in BD Difco Nutrient Broth (#234000) with 5 μg mL^{-1} tetracycline. All bacterial inoculations were incubated on a shaker at 37°C and 500 rpm. Growth curves for each strain were prepared under these conditions.

Incubation of cells with photosensitizer. Each 5 mL culture with a concentration of 1–3 × 10^8 CFU mL^{-1} (determined spectrophotometrically from the growth curve using a Genesys 10 UV scanning spectrophotometer from Thermo Electron Corp.) was pelleted by centrifugation (10 min, ~3700 ***g***) at 4°C, the supernatant discarded and the cells were resuspended in a total volume of 5 mL PBS (pH 7.2 with 0.05% Tween 80). A 1 mL aliquot of the bacterial solution was transferred to a separate culture tube to serve as a compound-free control. An appropriate volume of the CNC-Por (**1**) stock solution was added to the remaining 4 mL bacterial culture for a final concentration of 20 μM. The two tubes were wrapped in aluminum foil and were incubated for 5, 15, 30 or 60 min in the dark at room temperature and agitated by a vortex mixer set to the second lowest speed. Once the incubation was complete, three 1 mL aliquots from the culture tube containing the PS were placed in separate wells on a 24-well plate. The compound-free control (no compound control) and the remaining 1 mL culture containing CNC-Por (**1**) (PS-treated dark control) were placed in the dark while the plate underwent illumination.

Cell illumination conditions. All photosensitization experiments were performed using a noncoherent light source, Lumacare model LC122 (LumaCare), and the fluence rate was measured with an Orion power meter (Orphir Optronics Ltd, Israel) to measure the light intensity at the top (surface) and bottom of the assay plate. 1 mL aliquots of the cell suspension in PBS were added to a sterile 24 well plate (BD Falcon, flat bottom) and illuminated with visible light (400–700 nm) with a fluence rate of 65 mW cm^{-2} for the duration of 15 or 30 min (corresponding to fluences of 59 or 118 J cm^{-2}) while magnetically stirred (200 rpm). Tween-80 (0.05%) was added to the buffer to prevent excessive aggregation of the PS during the illumination process. After illumination, an aliquot was used for viability assays. All cell illumination experiments were conducted in triplicate at a minimum.

Cell survival assays. Once illumination was complete, 40 μL from each illuminated cell suspension, compound-free dark control, and compound-containing dark control, were 1:10 serially diluted in PBS six times and plated on square plates (LB–Miller broth-Agar plates for both *A. baumannii* and MDRAB, Difco Nutrient Broth-Agar plates for *P. aeruginosa*, and Tryptic Soy Broth-Agar plates for methicillin-resistant *S. aureus*) as described by Jett and coworkers (69). The plates were incubated at 37°C in the dark. The survival rate was determined from the ratio of CFU mL^{-1} of the illuminated solution and the no compound control. Because of the plating technique employed, a maximum of a 6 log unit change in CFU mL^{-1} corresponding to ≥100 CFU mL^{-1} could be detected for an initial concentration of 1 × 10^8 CFU mL^{-1}. Survival rates of < 0.0001% could not be detected. The percentage of survival for samples for which the corresponding plates did not show any colonies was thus set to the detection limit of 0.0001%. Samples with PS present but kept in the dark (dark control) served as a control. Statistical significance was assessed via a two-tailed, unpaired Student's *t*-test.

Confocal fluorescence microscopy of CNC-Por (1). Confocal fluorescence microscopy was performed on a Zeiss 710 LSM (Cellular and Molecular Imaging Facility, NCSU). All experiments were performed with *Acinetobacter baumannii* and *S. aureus* at concentrations comparable with the cell survival assays. Bacterial samples were prepared with and without PS, using either the precursor porphyrin Zn-EpPor (**3**) (Fig. 1) in solution or CNC-Por (**1**) as the PS. All concentrations, incubation times, and illumination times were comparable to those performed during the PDI survival assays. To eliminate as many variables as possible, two *A. baumannii* samples were grown simultaneously in culture tubes until reaching 1–3 × 10^8 CFU mL^{-1}. The bacteria were pelleted via centrifugation and resuspended in PBS buffer. CNC-Por (**1**) was then added to one culture tube, while Zn-EpPor (**3**) was added to the other at equal concentration. The tube with CNC-Por (**1**) as the PS was placed on a vortexer in the dark for 30 min, while the tube containing the Zn-EpPor (**3**) was placed on an orbital shaker (400 rpm) at 37°C also in the dark. A 1 mL aliquot of the PS-incubated cells was transferred to a well on a 24-well plate and illuminated for 30 min, after which a sample from each well was then prepared per standard microscopy protocols and imaged. Excitation was performed using an Argon laser at 458 nm at a quarter of its maximal intensity, and the intrinsic porphyrin fluorescence was observed. All images were obtained under identical conditions (pinhole, gain, filters) for comparison purposes.

RESULTS

Preparation and UV–visible spectroscopic characterization of CNC-Por (1)

CNC-Por (**1**) and its benzoylated derivative, **1-Bz**, were prepared as previously described (Fig. 1) (67). Treatment of CNC-Por (**1**) with benzoyl chloride in the ionic liquid 1-allyl-3-methylimidazolium chloride resulted in the benzoylated derivative of CNC-Por, **1-Bz**, thus rendering the normally insoluble

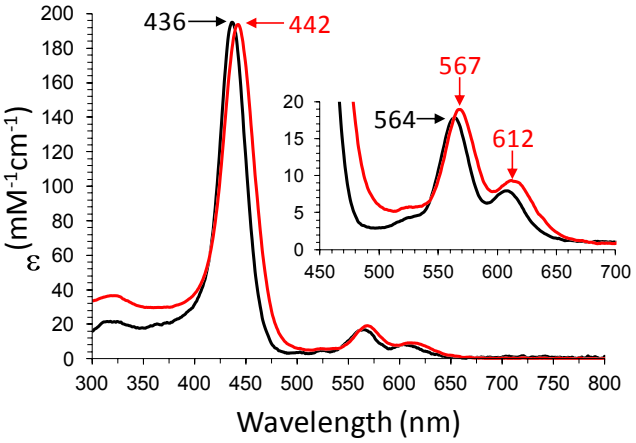

Figure 2. Electronic absorption spectra of benzoylated CNC-Por (**1-Bz**) (red) and the water-soluble precursor porphyrin Zn-EpPor (**3**) (black) in 30:1 H_2O:DMSO solution.

cellulosic material soluble in organic and aqueous solvents for subsequent characterization by UV–visible spectroscopy. The electronic absorption spectrum of **1-Bz** in H_2O:DMSO (30:1) (Fig. 2) exhibits spectral features [UV–visible: 442 (Soret), 567, 612 nm] that are typical for a Zn-metallated porphyrin of the tris-(4-methylpyridin-4-ium-1-yl) scaffold such as that employed in CNC-Por (**1**) (68). When compared with the spectrum of Zn-EpPor (**3**) [UV–visible: 436 (Soret), 564, 608 nm] obtained under identical conditions, **1-Bz** exhibits bathochromic shifts that are likely attributable to the differences in the local environment (e.g. polarity and solvation) of the porphyrin because of the presence of the covalently appended cellulose. Notably, the free-base (unmetallated) precursor, EpPor, exhibits spectral features [UV–visible: 426 (Soret), 521, 557, 591 and 648 nm] (68) that are distinct from **1-Bz** and its Zn-metallated analog under similar conditions. As **1-Bz** does not exhibit a hypsochromic shift of its Soret band that is indicative of the free-base porphyrin, the UV–visible spectroscopic data strongly support a fully metallated porphyrin (i.e. 1:1 Zn:porphyrin stoichiometry) in CNC-Por (**1**). Additional characterization of both CNC-Por (**1**) and Zn-EpPor (**3**) by solid-state UV–visible spectroscopy is provided in Figure S1.

Photodynamic inactivation studies with CNC-Por (1)

The photobactericidal activity of CNC-Por (**1**) was investigated using *A. baumannii*, multidrug resistant *A. baumannii* (MDRAB), methicillin-resistant *S. aureus* and *P. aeruginosa*. As supported by the UV–visible characterization of the porphyrin-cellulose nanocrystals (*vide supra*), a 1:1 zinc-to-porphyrin stoichiometry was assumed which enabled the porphyrin loading of the stock solution of CNC-Por (**1**) to be determined by a direct measurement of zinc ion concentration using ICP-mass spectrometry. Thus, the 20 μM concentration of CNC-Por (**1**) employed refers to the concentration of the porphyrin on CNC-Por (**1**) present in the suspension. Control experiments included survival assays of the bacteria in PBS buffered solution kept in the dark in the absence (no compound dark control) and presence (PS-treated dark control) of CNC-Por (**1**). The percentage of cell survival was calculated as the ratio of the colony count from PS-treated

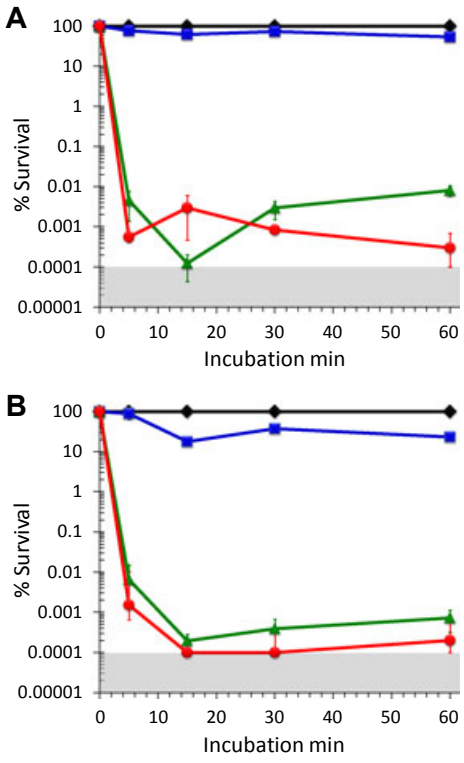

Figure 3. Photodynamic inactivation of (A) *A. baumannii* and (B) MDRAB using 20 μM CNC-Por (**1**) as the photosensitizer. The dark incubation time was varied over 5, 15, 30 and 60 min. Displayed is the % survival in PBS buffered bacterial suspensions for the compound-free dark control (♦), CNC-Por dark control (■) and light-treated samples after illumination times of 15 (▲) or 30 (●) min (total fluences of 59, and 118 J cm^{-2}, respectively, at 65 mW cm^{-2}). As the plating technique employed to determine % survival did not allow for detection of survival rates of $<0.0001\%$, data points below the detection limit are set to 0.0001% survival for graphing purposes. The shaded areas correspond to undetectable cell survival with the assay employed. In the cases where error bars cannot be visualized, the error bars themselves were smaller than the marker employed in the plot.

illuminated cultures and the no compound dark control, the latter being set to 100% survival in Figs. 3–5.

Acinetobacter baumannii and MDRAB. The results for the photodynamic inactivation of *A. baumannii* and MDRAB are shown in Figs 3A,B, respectively. For the PS-treated dark control, *A. baumannii* exhibited upwards of 0.4 log units reduction in CFUs ($P = 0.002$), indicative of a minor amount of dark toxicity of CNC-Por (**1**) against this bacterium (Fig. 3A). Upon illumination for 15 min, however, a more significant and clear loss in viable cells for *A. baumannii* was noted. Within error, the 5, 30, and 60 min dark incubation times each achieved a ~4.5 log units reduction in CFUs ($P < 0.0001$). As an outlier, the 15 min dark incubation time showed an unexpected, yet reproducible, 6 log units reduction when illuminated for 15 min, the origin of which was not explored further. Increasing the illumination period to 30 min resulted in a statistically significant ($P < 0.03$) improvement in the inactivation of *A. baumannii* to 4.5–5.5 log units reduction in viable cells (with the exception of the 15 min dark incubation time as noted above). Comparison of the 30 min illumination data again revealed no statistically significant dependence of survival as a function of dark incubation time.

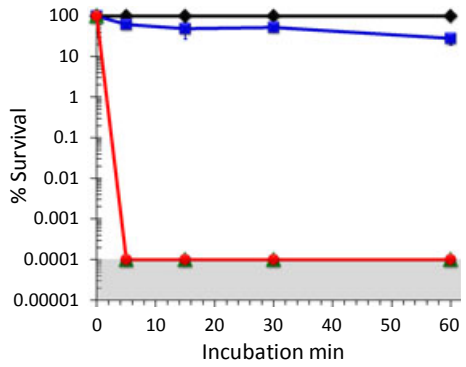

Figure 4. Photodynamic inactivation of methicillin-resistant *S. aureus* using 20 μM CNC-Por (**1**) as the photosensitizer. Displayed is the % survival in PBS-buffered bacterial suspensions for the compound-free dark control (♦), CNC-Por dark control (■) and light-treated samples after illumination times of 15 (▲) or 30 (●) min. Assay conditions were as specified in Fig. 3. Note: *A. baumannii* exhibits, and can interconvert between, both bacillar and coccoid morphologies (79).

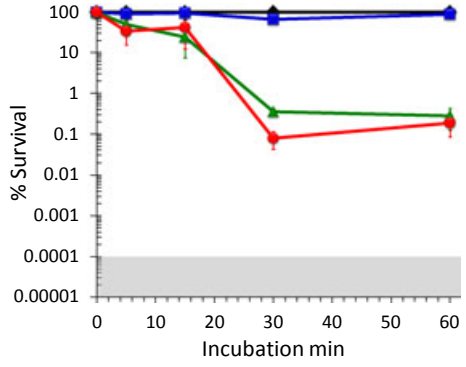

Figure 5. Photodynamic inactivation of *P. aeruginosa* using 20 μM CNC-Por (**1**) as the photosensitizer. Displayed is the % survival in PBS buffered bacterial suspensions for the compound-free dark control (♦), CNC-Por dark control (■) and light-treated samples after illumination times of 15 (▲) or 30 (●) min. Assay conditions were as specified in Fig. 3.

MDRAB exhibited dark toxicity (upwards of ~0.7 log units) that was more apparent at incubation times greater than 15 min (Fig. 3B). As was observed for *A. baumannii*, illumination of the MDRAB culture for 15 min resulted in 4 log units reduction in CFUs ($P < 0.0001$) for the 5 min dark incubation, and greater than 5 log units reduction in viable cells when the dark incubation time was further lengthened (15–60 min). A statistically significant increase in inactivation by ~1 log unit more was observed when the illumination time was increased to 30 min. With a few exceptions at the extremes of the conditions studied (the results for the 5 min dark incubation data [both 15 and 30 min illuminations] and the 60 min dark incubation/30 min. illumination data were virtually identical between the two bacteria), MDRAB was statistically more susceptible ($P = \sim 0.02$ or lower), albeit only slightly, to photodynamic inactivation by CNC-Por (**1**) when compared with *A. baumannii*.

Methicillin-resistant Staphylococcus aureus *(MRSA)*. The photodynamic inactivation of methicillin-resistant *S. aureus* by CNC-Por (**1**) was found to be highly effective (Fig. 4) under all conditions examined. Regardless of the dark incubation time or the illumination period, no CFUs were detected, and survival rates were therefore below the detection limit of $< 0.0001\%$, corresponding to an impressive 6 log units reduction in viable cells ($P < 0.0001$). Dark controls of the PS-treated cultures containing CNC-Por (**1**) showed at most 0.5 log units reduction in CFUs at the longer dark incubation times. *S. aureus*, being a Gram-positive bacterium, lacks an outer cell membrane, and it is likely for this reason that *S. aureus* is so highly susceptible to the cytotoxic species produced during the photodynamic inactivation process.

Pseudomonas aeruginosa. In comparison to the other bacterial strains investigated, *P. aeruginosa* appeared to be the least susceptible to photodynamic inactivation by CNC-Por (**1**) (Fig. 5). No statistically significant inactivation of *P. aeruginosa* was observed when incubated for less than 30 min. When the incubation was 30 or 60 min, a 2.5–3 log units reduction in the cell count was observed for both illumination times ($P < 0.0001$). Thus, the dark incubation time that preceded illumination did appear to play a role in the ability of CNC-Por (**1**) to mediate the photodynamic inactivation of *P. aeruginosa*, whereas the incubation time had no effect on the ability for CNC-Por (**1**) to inactivate *A. baumannii* or MRSA, and a minimal effect on MDRAB that was only observed for the 5 min dark incubation. No statistically significant dark toxicity on the survival of *P. aeruginosa* was attributed to CNC-Por (**1**).

Confocal fluorescence microscopy studies of *A. baumannii* and *S. aureus* with CNC-Por (1)

Confocal fluorescence microscopy was employed to investigate the interaction of CNC-Por (**1**) with *A. baumannii* (Fig. 6) prior to and after completion of a typical cell survival assay. Fluorescence was achieved by employing an excitation wavelength of 458 nm that was nearly coincident with the Soret absorbance of CNC-Por (**1**) (442 nm). *Acinetobacter baumannii* is a Gram-negative, encapsulated, pleomorphic bacterium that exhibits both bacillar and coccoid morphologies. Panel A depicts the size distribution of the cellulose-porphyrin nanocrystalline aggregates relative to the bacterium. Although individual cellulose nanocrystals (average length of 100–400 nm [66, 60] can be observed, the material formed aggregates that were generally much larger (~1–8 μm in length). Notably, as illustrated in panels B and C, no fluorescence was observed either internalized within *A. baumannii*, or localized to its cell membrane. Although this does not conclusively rule out a PS internalization mechanism or adherence of the PS to the cell membrane as the mechanism for bacterial PDI, it does suggest that the porphyrin of CNC-Por (**1**) remains covalently bound to the cellulose throughout the cell illumination assay and does not undergo degradation to form a water-soluble species. By contrast, as shown in panel D, the water-soluble porphyrin Zn-EpPor (**3**), when in solution and not bound to the cellulose nanocrystals, led to the fluorescence being localized on *A. baumannii*. Although the resolution of the confocal microscope did not allow for the determination of whether the cationic PS was internalized by the bacterium, or simply bound through an electrostatic interaction to the negatively charged bacterial cell membrane, the results highlight a stark contrast between how

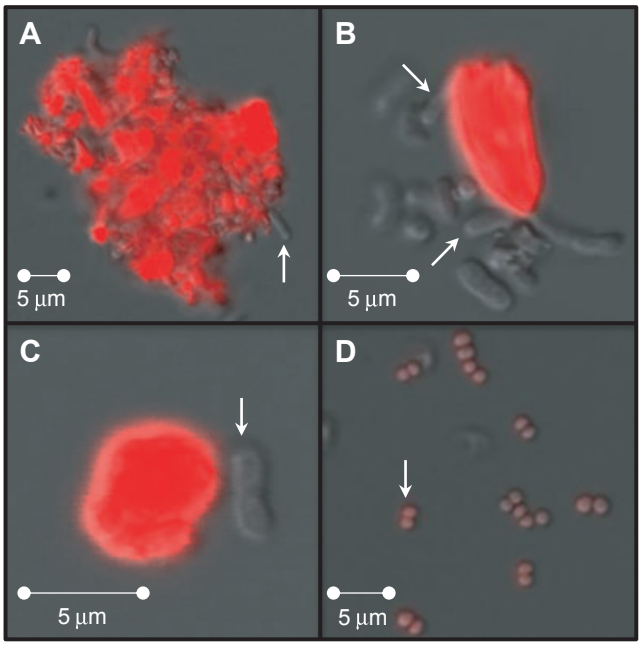

Figure 6. Confocal fluorescence microscopy images of *A. baumannii* acquired post illumination (30 min) in the presence of A-C) CNC-Por (**1**) and D) the solution-based Por photosensitizer. See text for additional details.

an insoluble PS such as CNC-Por (**1**) interacts with a bacterium when compared with a more traditional, solution-based PS.

Confocal fluorescence microscopy was also employed to investigate the interaction of CNC-Por (**1**) with *S. aureus* (Fig. 7). Panel A shows the observed fluorescence, panel B shows the corresponding light image, and panel C is the overlay of the fluorescence and light images. As was the case with *A. baumannii*, no fluorescence was observed either internalized within *S. aureus*, or localized to its cell membrane. Rather, the observed fluorescence is only coincident with the CNC-Por (**1**) material. These results are again consistent with the premise that the porphyrin-based PS of CNC-Por (**1**) remains covalently bound to the cellulose.

DISCUSSION

The attractiveness of cellulose as a bioavailable, biocompatible, biodegradable, and renewable scaffold for photobactericidal materials has recently garnered attention, particularly as it is amenable to the covalent attachment of PSs using current bioconjugation methodologies (21–23,29–31,70,71). Our focus has been on utilizing the unique properties and molecular control afforded by cellulose nanocrystals, allowing for well-defined, discrete nanodomains that have been derivatized with a variety of antimicrobial functional groups, and in particular with PSs, thereby allowing for fundamental and systematic investigations of the photoantibacterial efficacy of these systems. Our earlier work demonstrated the efficacy of the solution-based cationic PS TMPyP (meso-tetrakis[1-methyl-4-pyridinyl]porphyrin tetratosylate) in mediating the photodynamic inactivation of *M. smegmatis* (72). TMPyP has a reasonable quantum yield for singlet oxygen (0.74) (73), and our work with the singlet oxygen quencher NaN_3 demonstrated that the primary causative oxidative agent for the PDI of *M. smegmatis* was attributable to singlet oxygen, although other cytotoxic radical species may also play a role. Based on these results with TMPyP, we chose to covalently attach an alkyne-containing analogue, Zn-EpPor (**3**) (68), to azide-modified cellulose nanocrystals (66) using the Cu(I)-catalyzed Huisgen-Meldal-Sharpless 1,3-dipolar cycloaddition reaction (a "Click" reaction) (74,75), thereby forming the benchmark compound CNC-Por (**1**) (67). Along with characterizing CNC-Por (**1**) using nuclear magnetic resonance and infrared spectroscopies, as well as thermogravimetric analysis, gel permeation chromatography and other analytical methods, the photobactericidal properties of the porphyrin-cellulose nanocrystals were investigated, but in limited fashion. Our aim here is to provide supporting spectroscopic characterization of CNC-Por (**1**), and, moreover, to expand the breadth and scope of the antimicrobial study to include additional strains not previously investigated, including antibiotic-resistant ones.

In our previous study of CNC-Por (**1**) (67), the porphyrin loading was determined using atomic absorption spectroscopy, with the critical assumption being that the porphyrin was fully metallated with zinc (i.e. a 1:1 Zn:porphyrin stoichiometry was present). However, if full or even partial demetallation of the

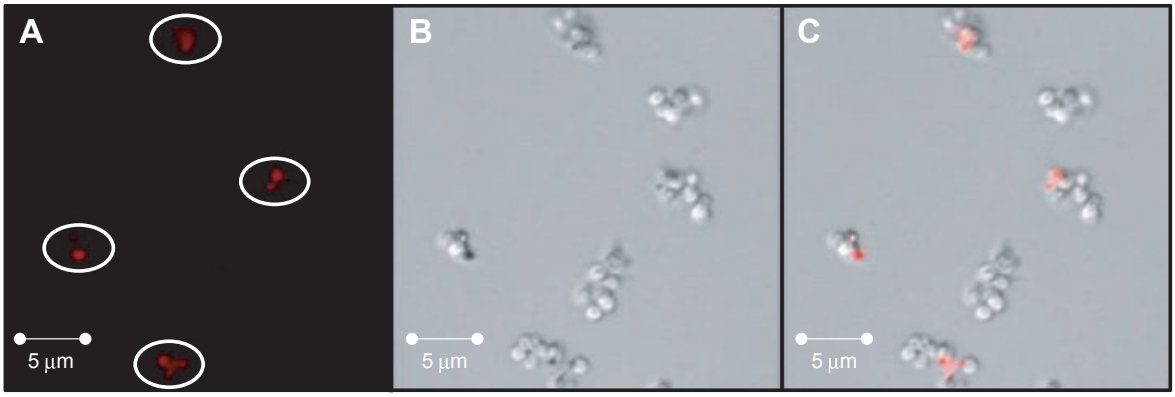

Figure 7. Confocal fluorescence microscopy images of *S. aureus* acquired post illumination (30 min) in the presence of CNC-Por (**1**). (A) Fluorescence image (458 nm excitation) depicting the location of the photosensitizer. (B) Light image showing the location of the *S. aureus* cells. (C) Overlay of the images in panels A and B.

porphyrin occurred during the synthesis of CNC-Por (**1**), this would result in an erroneously low value of porphyrin loading, thereby leading to the use of a higher concentration of CNC-Por (**1**) in the cell survival assays than desired, and thus an overstatement of the efficacy of the photobactericidal material. Thus, it was imperative to conclusively establish that no detectable demetallation of the porphyrin in CNC-Por (**1**) occurred during its synthesis and subsequent purification. To that end, CNC-Por (**1**) was benzoylated for improved solubility (67), and its solution UV–visible spectrum was obtained. The electronic absorption spectrum exhibited features that were consistent with a zinc-metallated porphyrin, and, importantly, it was not possible to observe any of the spectroscopic features attributable to a free-base (demetallated) porphyrin (hypsochromic shift of the Soret band and the presence of four Q bands). Given the >10 nm difference in the wavelength maxima of the Soret bands for the metallated and free-base porphyrins (68), and given the distinct Q band features for each, we estimate that CNC-Por (**1**) is minimally 95% metallated.

The extent of antimicrobial activity was examined for CNC-Por (**1**) as a function of bacterial strain, including *A. baumannii*, MDRAB, methicillin-resistant *S. aureus*, and *P. aeruginosa*. The best results demonstrated activity from a 2.5 log units reduction in viable cells for *P. aeruginosa* (60 min incubation, 30 min illumination, 99.7% cell inactivation, $P < 0.0001$) to a 6 log units reduction for MRSA (all conditions, 99.9999 + % cell loss, $P < 0.0001$). As was previously noted for *S. aureus* (67), the MRSA strain employed here appeared to be the most susceptible bacterium of those studied for bacterial PDI when mediated by CNC-Por (**1**). This result is not unexpected, however, as Gram-positive bacteria such as *S. aureus* lack an outer cell membrane, and possess a relatively more porous peptidoglycan cell wall that likely favors association with photosensitizers, thus rendering the bacterium more susceptible to damage from PDI (76). In contrast to the excellent results achieved with *S. aureus*, the maximum viable cell loss observed for the Gram-negative *P. aeruginosa*, although still significant at about 99.7%, was ~3.5 log units less, and required the longer incubation periods prior to illumination. One could attribute this observed difference in bacterial inactivation to the presence (Gram-negative) or absence (Gram-positive) of the outer bacterial cell wall. However, the other Gram-negative bacterial strains examined herein, *A. baumannii* and MDRAB, displayed a reduction in viable cells that, although intermediate between *S. aureus* and *P. aeruginosa*, was still nearly to the detection limit (~5–6 log units reduction). Our previous study investigating the inactivation of *E. coli* (Gram-negative) with CNC-Por (**1**) revealed a ~2 log units reduction in CFUs, whereas *M. smegmatis* (mycobacterium/Gram-positive) was inactivated up to 3.5 log units, and up to 6 log units inactivation was observed for methicillin-sensitive *S. aureus* (MSSA). Thus, while the lack of the outer cell wall likely plays a significant role in the inability of Gram positive bacteria to resist photobactericidal inactivation, other factors that have yet to be determined (e.g. differences in biofilm formation, the number of porin channels, cell morphology, etc., between bacterial strains) must also play significant roles in order to explain the variability in inactivation of the Gram-negative strains.

The photobactericidal activity of CNC-Por (**1**) was also examined as a function of light dose and dark incubation time. Not surprisingly, under nearly all conditions examined, the 30 min light dose achieved a greater reduction in viable cells than the 15 min light dose when a statistically significant difference between the two conditions was observed, and is likely attributable to the higher amount of cytotoxic reactive oxygen species, in particular $^1O_2$, formed during the increased illumination time. No cell survival dependence on dark incubation times was observed for *A. baumannii*, and a minimal effect was noted for MDRAB that was only observed for the 5 min dark incubation. Additionally, because of the complete inactivation of MRSA, no dark incubation time dependence could be observed with the detection limit utilized. Interestingly, however, a dependence on the dark incubation time was observed for *P. aeruginosa*, as statistically significant inactivation was only observed for the 30 and 60 min incubation times and not for the shorter ones. Previously, we also noted a dark incubation time dependence on the inactivation of *M. smegmatis* by CNC-Por (**1**), and at that time it was hypothesized that the action of putative endogenous mycobacterial cellulases may partially degrade CNC-Por (**1**), leading to the release of smaller, water-soluble porphyrin-polysaccharides that could lead to the observed increase in PDI efficiency at longer dark incubation times (67). However, to the best of our knowledge, there are no known cellulases of *P. aeruginosa*. A combination of other factors, such as preferential adherence of one bacterium over another to the porphyrin-cellulose nanocrystals caused by the differences in bacterial cell wall morphology, or possibly even the secretion of exopolysaccharide biofilms by specific bacteria, could lead to the observed dark incubation time dependencies. Additional studies are currently underway in our laboratory to elucidate the origin of the dark incubation time dependence on the antimicrobial PDI of *P. aeruginosa* and *M. smegmatis*.

To gain more insight into the bactericidal mechanism of CNC-Por (**1**), confocal fluorescence microscopy was employed to image the CNC-Por (**1**)-treated cultures of *A. baumannii* (Fig. 6) and *S. aureus* (Fig. 7). Qualitatively, both the bacterium and the porphyrin-cellulose nanocrystals were indistinguishable pre- and postillumination, suggesting that the morphology of the nanocrystalline material was unchanged despite having undergone a photodynamic process. Importantly, neither pre- nor postilluminated samples when treated with CNC-Por (**1**) exhibited evidence of porphyrin fluorescence either internalized within either *A. baumannii* or *S. aureus*, or localized on the bacterial cell surface. By contrast, when the bacteria were treated with the water-soluble Zn-EpPor (**3**), fluorescence was observed superimposed upon the bacterium, suggesting that the solution-based PS was either internalized or bound to the cell membrane. Taken together, the results support the hypothesis that direct binding and uptake of the PS are not necessary requirements for photodynamic inactivation by CNC-Por (**1**), and, as reactive oxygen species have been shown to diffuse over a wide range of distances (from <250 nm for $^1O_2$ to ~1.5 mm for H_2O_2) in aqueous solution (32–34), the production of $^1O_2$ and other cytotoxic or radical species in close proximity to the bacteria may be sufficient to result in cell inactivation or death. By the same token, in light of our previous observation that a 100- to 500-fold higher porphyrin concentration is needed for

CNC-Por (**1**) to photoinactivate *M. smegmatis* to the same extent when compared with soluble PSs [i.e. Zn-EpPor (**3**)] (67, 72), one can regard a diffusion-based process of cytotoxic species from the insoluble PS as being less effective than a direct interaction (internalization or localization of the PS to the bacterial cell membrane), the latter being what may be needed for effective aPDT at very low PS concentrations *in vivo*.

CONCLUSION

We have now further investigated the ability of CNC-Por (**1**) to photoinactivate bacteria of different genera using visible light (400–700 nm). An impressive 6 log units of reduction in viable cells was observed for methicillin-resistant *S. aureus* (Gram-positive), 5–6 log units for *A. baumannii* and MDRAB (Gram-negative), and ~2.5 log units for *P. aeruginosa* (Gram-negative) when using a 20 μM suspension of CNC-Por (**1**) and illuminated with visible light (400–700 nm) at a fluence of 118 J cm^{-2}. When viewed alongside our previous study which demonstrated that CNC-Por (**1**) was able to inactivate *S. aureus* (MSSA) by 5–6 log units reduction of viable cells, *M. smegmatis* by 3–4 log units, and *E. coli* by 1–2 log units under similar illumination conditions, it is possible to conclude that CNC-Por (**1**) is able to mediate the photodynamic inactivation of these strains of bacteria despite their variation in taxonomic classification. Confocal microscopy demonstrated that the mode of action for CNC-Por (**1**) likely does not proceed through a PS-binding or uptake mechanism. Rather, the cytotoxic species (e.g. $^1O_2$ and other reactive oxygen species) generated by the photodynamic process likely diffuses over short distances to ultimately damage the bacterium, leading to cell inactivation or death. This contrasts with Zn-EpPor (**3**), which as a solution-based PS was shown to directly interact with the bacteria (either internalized or localized to the cell membrane), and provides insight into the mode of action of soluble PSs *vs.* photobactericidal materials. Given the potential shown by this one cellulose–porphyrin conjugate to rapidly photoinactivate the five bacterial strains examined to date with moderate to high efficiency, future efforts will focus on a number of different areas, including biological, photophysical, and synthetic investigations. To complement the solution studies performed to date, the potential for the effective inactivation of bacteria on dry surfaces (such as filters) coated with CNC-Por (**1**) will be examined as it has been shown that $^1O_2$ is able to diffuse over distances as long as 1 mm in air (77). Studies investigating the effect of CNC-Por (**1**) on eukaryotic (e.g. epithelial) cells will also be of interest, particularly in light of a recent report that has shown putative antitumor efficacy of a related compound, chlorin-modified cellulose nanocrystals, against human keratinocyte HaCat cells with IC_{50} values in the nanomolar range (78). The photophysical properties (quantum yields of $^1O_2$ and radical production) of CNC-Por (**1**) will also be determined, as will be the effects of fluence and concentration on the PDI efficiency. Additional, future efforts will focus on the systematic modification of the porphyrin (e.g. charge, hydrophobicity, meso-substituents) to create a library of PS-cellulose nanocrystalline systems that will allow for elucidating the fundamental interactions that govern PDI of bacteria through these cellulose derivatives, while at the same time leading to the development of potent photobactericidal materials with broad spectrum antimicrobial activity to combat the growing threat to human health posed by the transmission of pathogenic bacteria.

Acknowledgements—This project was supported with funds from North Carolina State University (R.A.G and D.S.A.) as well as funds from the Finnish funding agency for Technology & Innovation; Tekes (D.S.A.). We also gratefully acknowledge Prof. Paul Maggard (North Carolina State University) for help in obtaining the solid-state UV–visible spectra of CNC-Por (**1**) and Zn-EpPor (**3**).

SUPPORTING INFORMATION

Additional Supporting Information may be found in the online version of this article:

Figure S1. Solid state UV–visible Spectra of (A) CNC-Por (**1**) and (B) Zn-EpPor (**3**)

Please note: Wiley-Blackwell is not responsible for the content or functionality of any supporting information supplied by the authors. Any queries (other than missing material) should be directed to the corresponding author for the article.

REFERENCES

1. Scott, R. D.. (2009) *The Direct Medical Costs of Healthcare-Associated Infections in U.S. Hosptials and the Benefits of Prevention*, p. 13. Centers for Disease Control and Prevention, Atlanta, GA.
2. Jawad, A., A. M. Snelling, J. Heritage and P. M. Hawkey (1998) Exceptional desiccation tolerance of Acinetobacter radioresistens. *J. Hosp. Infect.* **39**, 235–240.
3. Hirai, Y. (1991) Survival of bacteria under dry conditions; from a viewpoint of nosocomial infection. *J. Hosp. Infect.* **19**, 191–200.
4. Guenthner, S. H., J. O. Hendley and R. P. Wenzel (1987) Gram-negative bacilli as nontransient flora on the hands of hospital personnel. *J. Clin. Microbiol.* **25**, 488–490.
5. Kramer, A., I. Schwebke and G. Kampf (2006) How long do nosocomial pathogens persist on inanimate surfaces? A systematic review *BMC Infect. Dis.* **6**, 130.
6. Demidova, T. N. and M. R. Hamblin (2004) Photodynamic therapy targeted to pathogens. *Int. J. Immunopathol. Pharmacol.* **17**, 245–254.
7. Hamblin, M. R. and T. Hasan (2004) Photodynamic therapy: A new antimicrobial approach to infectious disease? *Photochem. Photobiol. Sci.* **3**, 436–450.
8. Dai, T., Y. Y. Huang and M. R. Hamblin (2009) Photodynamic therapy for localized infections – State of the art. *Photodiagn. Photodyn. Ther.* **6**, 170–188.
9. Capella, M., A. M. Coelho and S. Menezes (1996) Effect of glucose on photodynamic action of methylene blue in Escherichia coli cells. *Photochem. Photobiol.* **64**, 205–10.
10. Menezes, S., M. A. Capella and L. R. Caldas (1990) Photodynamic action of methylene blue: Repair and mutation in Escherichia coli. *J. Photochem. Photobiol., B* **5**, 505–17.
11. Reddi, E., M. Ceccon, G. Valduga, G. Jori, J. C. Bommer, F. Elisei, L. Latterini and U. Mazzucato (2002) Photophysical properties and antibacterial activity of meso-substituted cationic porphyrins. *Photochem. Photobiol.* **75**, 462–470.
12. Valduga, G., B. Breda, G. M. Giacometti, G. Jori and E. Reddi (1999) Photosensitization of wild and mutant strains of Escherichia coli by meso-tetra (N-methyl-4-pyridyl)porphine. *Biochem. Biophys. Res. Commun.* **256**, 84–88.
13. Konig, K., M. Teschke, B. Sigusch, E. Glockmann, S. Eick and W. Pfister (2000) Red light kills bacteria via photodynamic action. *Cell. Mol. Biol.* **46**, 1297–1303.
14. Merchat, M., J. D. Spikes, G. Bertoloni and G. Jori (1996) Studies on the mechanism of bacteria photosensitization by meso-substituted cationic porphyrins. *J. Photochem. Photobiol. B: Biol.* **35**, 149.

15. Bertoloni, G., F. Rossi, G. Valduga, G. Jori and J. van. Lier (1990) Photosensitizing activity of water- and lipid-soluble phthalocyanines on Escherichia coli. *FEMS Microbiol. Lett.* **59**, 149–155.
16. Nitzan, Y., M. Gutterman, Z. Malik and B. Ehrenberg (1992) Inactivation of gram-negative bacteria by photosensitized porphyrins. *Photochem. Photobiol.* **55**, 89–96.
17. Merkel, P. B. and D. R. Kearns (1972) Radiationless decay of singlet molecular oxygen in solution Experimental and theoretical study of electronic-to-vibrational energy transfer. *J. Am. Chem. Soc.* **94**, 7244–7253.
18. Maisch, T. (2007) Revitalized strategies against multidrug-resistant bacteria: Anti-microbial photodynamic therapy and bacteriophage therapy. *Anti-Infect. Agents Med. Chem.* **6**, 145.
19. Embleton, M. L., S. P. Nair, B. D. Cookson and M. Wilson (2004) Antibody-directed photodynamic therapy of methicillinresistant Staphylococcus aureus. *Microb. Drug Resist.* **10**, 92.
20. Embleton, M. L., S. P. Nair, W. Heywood, D. C. Menon, B. D. Cookson and M. Wilson (2005) Development of a novel targeting system for lethal photosensitization of antibiotic-resistant strains of Staphylococcus aureus. *Antimicrob. Agents Chemother.* **49**, 3690–3696.
21. Krouit, M., R. Granet, P. Branland, B. Verneuil and P. Krausz (2006) New photoantimicrobial films composed of porphyrinated lipophilic cellulose esters. *Bioorg. Med. Chem. Lett.* **16**, 1651–1655.
22. Krouit, M., R. Granet and P. Krausz (2008) Photobactericidal plastic films based on cellulose esterified by chloroacetate and a cationic porphyrin. *Bioorg. Med. Chem.* **16**, 10091–10097.
23. Krouit, M., R. Granet and P. Krausz (2009) Photobactericidal films from porphyrins grafted to alkylated cellulose – Synthesis and bactericidal properties. *Eur. Polym. J.* **45**, 1250–1259.
24. Bonnett, R., M. A. Krysteva, I. G. Lalov and S. V. Artarsky (2006) Water disinfection using photosensitizers immobilized on chitosan. *Water Res.* **40**, 1269–1275.
25. Wilson, M. (2003) Light-activated antimicrobial coating for the continuous disinfection of surfaces. *Infect. Control Hosp. Epidemiol.* **24**, 782–784.
26. Sherrill, J., S. Michielsen and I. Stojiljkovic (2003) Grafting of light-activated antimicrobial materials to nylon films. *J. Polym. Sci., A: Polym. Chem.* **41**, 41–47.
27. Lucas, R., R. Granet, V. Sol, C. L. Morvan, C. Policar, E. Riviere and P. Krausz (2007) Synthesis and cellular uptake of superparamagnetic dextran-nanoparticles with porphyrinic motifs grafted ob esterification. *e-Polymers* **89**, 1–8.
28. Carvalho, C. M. B., E. Alves, L. Costa, J. P. C. Tome, M. A. F. Faustino, M. G. P. M. S. Neves, A. C. Tome, J. A. S. Cavaleiro, A. Almeida, A. Cunha, Z. Lin and J. Rocha (2010) Functional cationic nanomagnet – Porphyrin hybrids for the photoinactivation of microorganisms. *ACS Nano* **4**, 7133–7140.
29. Ringot, C., V. Sol, R. Granet and P. Krausz (2009) Porphyrin-grafted cellulose fabric: New photobactericidal material obtained by "Click-Chemistry" reaction. *Mater. Lett.* **63**, 1889–1891.
30. Ringot, C., N. Saad, R. Granet, P. Bressollier, V. Sol and P. Krausz (2010) *Meso*-functionalized aminoporphryins as efficient agents for photo-bactericidal surfaces. *J. Porphyrins Phthalocyanines* **14**, 925–931.
31. Ringot, C., V. Sol, M. Barriere, N. Saad, P. Bressollier, R. Granet, P. Couleaud, C. Frochot and P. Krausz (2011) Triazinyl porphyrin-based photoactive cotton fabrics: Preparation, characterization, and antibacterial activity. *Biomacromolecules* **12**, 1716–1723.
32. Midden, W. R. and S. Y. Wang (1983) Singlet oxygen generation for solution kinetics: Clean and simple. *J. Am. Chem. Soc.* **105**, 4129–4135.
33. Redmond, R. W. and I. E. Kochevar (2006) Spatially resolved cellular responses to singlet oxygen. *Photochem. Photobiol.* **82**, 1178–1186.
34. Winterbourn, C. C. (2008) Reconciling the chemistry and biology of reactive oxygen species. *Nat. Chem. Biol.* **4**, 278–286.
35. Lienkamp, K. and G. N. Tew (2009) Synthetic mimics of antimicrobial peptides – A versatile ring-opening metathesis polymerization based platform for the synthesis of selective antibacterial and cell-penetrating polymers. *Chemistry* **15**, 11784–11800.
36. Tew, G. N., D. Liu, B. Chen, R. J. Doerksen, J. Kaplan, P. J. Carroll, M. L. Klein and W. F. DeGrado (2002) De novo design of biomimetic antimicrobial polymers. *Proc. Natl Acad. Sci. USA* **99**, 5110–5114.
37. Haynie, S. L., G. A. Crum and B. A. Doele (1995) Antimicrobial activities of amphiphilic peptides covalently bonded to a water-insoluble resin. *Antimicrob. Agents Chemother.* **39**, 301–307.
38. Glinel, K., A. M. Jonas, T. Jouenne, J. Leprince, L. Galas and W. T. Huck (2009) Antibacterial and antifouling polymer brushes incorporating antimicrobial peptide. *Bioconjugate Chem.* **20**, 71–77.
39. Kurt, P., L. Wood, D. E. Ohman and K. J. Wynne (2007) Highly effective contact antimicrobial surfaces via polymer surface modifiers. *Langmuir* **23**, 4719–4723.
40. Cen, L., K. G. Neoh and E. T. Kang (2003) Surface functionalization technique for conferring antibacterial properties to polymeric and cellulosic surfaces. *Langmuir* **19**, 10295–10303.
41. Vigo, T. L.. (1994) Advances in antimicrobial polymers and materials. In *Biotechnology and Bioactive Polymers* (Edited by C. G. Gebelein and C. E. Carraher), p. 225. Plenum Press, New York.
42. Krishnan, S., R. J. Ward, A. Hexemer, K. E. Sohn, K. L. Lee, E. R. Angert, D. A. Fischer, E. J. Kramer and C. K. Ober (2006) Surfaces of fluorinated pyridinium block copolymers with enhanced antibacterial activity. *Langmuir* **22**, 11255–11266.
43. Viscardi, G., P. Quagliotto, C. Barolo, P. Savarino, E. Barni and E. Fisicaro (2000) Synthesis and surface and antimicrobial properties of novel cationic surfactants. *J. Org. Chem.* **65**, 8197–8203.
44. Kenawy, E.-R., F. I. Abdel-Hay, A. E.-R. R. El-Shanshoury and M. H. El-Newehy (2002) Biologically active polymers. V. Synthesis and antimicrobial activity of modified poly(glycidyl methacrylate-co-2-hydroxyethyl methacrylate) derivatives with quaternary ammonium and phosphonium salts. *J. Polym. Sci., A: Polym. Chem.* **40**, 2384–2393.
45. Kanazawa, A. and T. Ikeda (2000) Multifunctional tetracoordinate phosphorus species with high self-organizing ability. *Coord. Chem. Rev.* **198**, 117–131.
46. Vigo, T. L. (1992) Antimicrobial fibers and polymers. In *Manmade Fibers: Their Origin and Development* (Edited by R. B. Seymour and R. S. Porter), p. 214. Elsevier, Amsterdam.
47. Bromberg, L. and T. A. Hatton (2007) Poly(N-vinylguanidine): Characterization, and catalytic and bactericidal properties. *Polymer* **48**, 7490–7498.
48. Liang, J., Y. Chen, X. Ren, R. Wu, K. Barnes, S. D. Worley, R. M. Broughton, U. Cho, H. Kocer and T. S. Huang (2007) Fabric treated with antimicrobial N-halamine epoxides. *Ind. Eng. Chem. Res.* **46**, 6425–6429.
49. Eknoian, M. W., S. D. Worley, J. Bickert and J. F. Williams (1999) Novel antimicrobial N-halamine polymer coatings generated by emulsion polymerization. *Polymer* **40**, 1367–1371.
50. Chen, L., L. Bromberg, T. A. Hatton and G. C. Rutledge (2008) Electrospun cellulose acetate fibers containing chlorhexidine as a bactericide. *Polymer* **49**, 1266.
51. Ignatova, M., D. Labaye, S. Lenoir, D. Strivay, R. Jerome and C. Jerome (2003) Immobilization of silver in polypyrrole/polyanion composite coatings: Preparation, characterization, and antibacterial activity. *Langmuir* **19**, 8971–8979.
52. Estevao, L. R. M., L. C. S. Mendonca-Hagler and R. S. V. Nascimento (2003) Development of polyurethane antimicrobial composites using waste oil refinery catalyst. *Ind. Eng. Chem. Res.* **42**, 5950–5953.
53. Wainwright, M. (2003) Local treatment of viral disease using photodynamic therapy. *Int. J. Antimicrob. Agents* **21**, 510.
54. Santus, R., P. Grellier, J. Schrevel, J. C. Maziere and J. F. Stoltz (1998) Photodecontamination of blood components: Advantages and drawbacks. *Clin. Hemorheol. Microcirc.* **18**, 299–308.
55. Friedberg, J. S., C. Skema, E. D. Baum, J. Burdick, S. A. Vinogradov, D. F. Wilson, A. D. Horan and I. Nachamkin (2001) In vitro effects of photodynamic therapy on Aspergillus fumigatus. *J. Antimicrob. Chemother.* **48**, 105–7.
56. Donnelly, R. F., P. A. McCarron and M. M. Tunney (2008) Antifungal photodynamic therapy. *Microbiol. Res.* **163**, 1–12.
57. Grellier, P., R. Santus, E. Mouray, V. Agmon, J.-C. Maziere, D. Rigomier, A. Dagan, S. Gatt and J. Schrevel (1997) Photosensitized inactivation of plasmodium falciparum- and babesia

divergens-infected erythrocytes in whole blood by lipophilic pheophorbide derivatives. *Vox Sang*. **72**, 211–220.
58. Jori, G. (2007) Inactivation of pathogenic microorganisms by photodynamic techniques: Mechanistic aspects and perspective applications. *Anti-Infect. Agents Med. Chem*. **6**, 119–131.
59. Jori, G. and S. B. Brown (2004) Photosensitized inactivation of microorganisms. *Photochem. Photobiol. Sci*. **3**, 403–405.
60. Habibi, Y., L. A. Lucia and O. J. Rojas (2010) Cellulose nanocrystals: chemistry, self-assembly, and applications. *Chem. Rev*. **110**, 3479–3500.
61. Araki, J., M. Wada, S. Kuga and T. Okano (1999) Influence of surface charge on viscosity behavior of cellulose microcrystal suspension. *J. Wood Sci*. **45**, 258–261.
62. Araki, J., M. Wada, S. Kuga and T. Okano (1998) Flow properties of microcrystalline cellulose suspension prepared by acid treatment of native cellulose. *Colloids Surf. Physicochem. Eng. Aspects* **142**, 75–82.
63. Beck-Candanedo, S., M. Roman and D. G. Gray (2005) Effect of reaction conditions on the properties and behavior of wood cellulose nanocrystal suspensions. *Biomacromolecules* **6**, 1048–54.
64. Filpponen, I. (2009) *The Synthetic Strategies for Unique Properties in Cellulose Nanocrystals Materials*. Ph.D. thesis, North Carolina State University, Raleigh.
65. Ranby, B. G. (1951) Fibrous macromolecular systems. Cellulose and muscle. The colloidal properties of cellulose micelles. *Discuss. Faraday Soc*. **11**, 158–164.
66. Filpponen, I. and D. S. Argyropoulos (2010) Regular linking of cellulose nanocrystals via click chemistry: Synthesis and formation of cellulose nanoplatelet gels. *Biomacromolecules* **11**, 1060–1066.
67. Feese, E., H. Sadeghifar, H. S. Gracz, D. S. Argyropoulos and R. A. Ghiladi (2011) Photobactericidal porphyrin-cellulose: Nanocrystals synthesis, characterization, and antimicrobial properties. *Biomacromolecules* **11**, 3528–3539.
68. Feese, E.. (2011) *Development of Novel Photosensitizers for Photodynamic Inactivation of Bacteria*. Ph.D. thesis, North Carolina State University, Raleigh.
69. Jett, B. D., K. L. Hatter, M. M. Huycke and M. S. Gilmore (1997) Simplified agar plate method for quantifying viable bacteria. *Biotechniques* **23**, 648–650.
70. Holzer, W., A. Penzkofer, F. X. Redl, M. Lutz and J. Daub (2002) Excitation energy density dependent fluorescence behaviour of a regioselectively functionalized tetraphenylporphyrin-cellulose conjugate. *Chem. Phys*. **282**, 89–99.
71. Redl, F. X., M. Lutz and J. Daub (2001) Chemistry of porphyrin-appended cellulose strands with a helical structure: Spectroscopy, electrochemistry, and in situ circular dichroism spectroelectrochemistry. *Chem. Eur. J*. **7**, 5350–5358.
72. Feese, E. and R. A. Ghiladi (2009) Highly efficient in vitro photodynamic inactivation of Mycobacterium smegmatis. *J. Antimicrob. Chemother*. **64**, 782–785.
73. Wilkinson, F., W. P. Helman and A. B. Ross (1993) Quantum yields of photosensitized formation of the lowest electronically excited singlet state of molecular oxygen in solution. *J. Phys. Chem. Ref. Data* **22**, 113.
74. Tornoe, C. W., C. Christensen and M. Meldal (2002) Peptidotriazoles on solid phase: [1,2,3]-triazoles by regiospecific copper(I)-catalyzed 1,3-dipolar cycloadditions of terminal alkynes to azides. *J. Org. Chem*. **67**, 3057–3064.
75. Rostovtsev, V. V., L. G. Green, V. V. Fokin and K. B. Sharpless (2002) A stepwise huisgen cycloaddition process: copper(I)-catalyzed regioselective ''ligation'' of azides and terminal alkynes. *Angew. Chem. Int. Ed*. **41**, 2596–2599.
76. Navarre, W. W. and O. Schneewind (1999) Surface proteins of gram-positive bacteria and mechanisms of their targeting to the cell wall envelope. *Microbiol. Mol. Biol. Rev*. **63**, 174–229.
77. Dahl, T. A., W. R. Midden and P. E. Hartman (1987) Pure singlet oxygen cytotoxcity for bacteria. *Photochem. Photobiol*. **46**, 345–352.
78. Drogat, N., R. Granet, V. Sol, C. Le Morvan, G. Begaud-Grimaud, F. Lallouet and P. Krausz (2011) O108: Cellulose nanocrystals: A new chlorin carrier designed for photodynamic therapy: Synthesis, characterization and potent anti-tumoural activity. *Photodiagn. Photodyn. Ther*. **8**, 157.
79. James, G. A., D. R. Korber, D. E. Caldwell and J. W. Costerton (1995) Digital image analysis of growth and starvation responses of a surface-colonizing Acinetobacter sp. *J. Bacteriol*. **177**, 907–915.